

Counterstreaming Beams and Flat-Top Electron Distributions Observed with Langmuir, Whistler, and Compressional Alfvén Waves in Earth's Magnetic Tail

Alexandra Teste* and George K. Parks

Space Sciences Laboratory, University of California, Berkeley, 94720-7450 California, USA

(Received 26 November 2008; published 20 February 2009)

Relevant new clues to wave-particle interactions have been obtained in Earth's plasma sheet (PS). The plasma measurements made on Cluster spacecraft show that broadband ($\sim 2\text{--}6$ kHz) electrostatic emissions, in the PS boundary layer, are associated with cold counterstreaming electrons flowing at $5\text{--}12 \times 10^3$ km s $^{-1}$ through hot Maxwellian plasma. In the current sheet (CS), electromagnetic whistler mode waves ($\sim 10\text{--}80$ Hz) and compressional Alfvén waves (< 2 Hz) are detected with flat-topped electron distributions whose cutoff speeds are $\sim 15\text{--}17 \times 10^3$ km s $^{-1}$. These waves are damped in the central CS where $|B| \leq 1.5$ nT, plasma $\beta \sim 100$, and electron distributions isotropic. Three mechanisms are at work: the β -dependent lower hybrid drift instability (LHDI), acceleration of electrons along the B field by the LHD waves and whistler mode emissions triggered by the cyclotron resonance instability.

DOI: 10.1103/PhysRevLett.102.075003

PACS numbers: 94.30.cq, 94.05.Pt, 94.30.cl, 94.30.ct

Introduction.—Electron beams are ubiquitous and observed throughout the plasma Universe, in the Earth's ionosphere and magnetosphere [1,2], the solar corona [3] and pulsars [4]. These beams can excite electrostatic [5] and electromagnetic [6] waves important for accelerating particles in stars [7] and heating plasmas [8].

The waves observed in the Earth's magnetic tail have been studied the most and are best characterized. However, the mechanisms that produce these waves remain poorly understood [9]. Most studies in the past have focused on either waves or particles. Only one study included both [10]. However, the plasma measurements used in this study did not have sufficient time resolution to establish the detailed relationships between waves and particles needed to identify their interaction mechanisms.

Particle instruments on Cluster can obtain full three-dimensional (3D) plasma distribution in one spin (4 s), sufficient to reveal the details of how the electron distribution functions behave and evolve in the different layers of the plasma sheet (PS), not previously possible. Plasma data obtained concurrently with wave measurements have now revealed that the broadband electrostatic (ES) waves in the plasma sheet boundary layer occur in the presence of cold counterstreaming electron beams flowing through hot Maxwellian distributions, different from the bump-in-tail distribution as previously thought. Closer to the equator in the current sheet, the electromagnetic (EM) whistler mode and compressional Alfvén waves occur with flat-top electron distributions. The distributions become Maxwellian and the whistler mode waves are damped in the central current sheet (neutral sheet) where the ion plasma $\beta_i = 2\mu_0 N k_B T / B^2 \sim 100$ and ions are unmagnetized. The neutral sheet is ~ 300 km thick, much smaller than the ion Larmor radius of typical 5 keV protons that populate the PS (~ 7000 km).

A combination of instability mechanisms is apparently responsible for these observations. First, we note that large density and temperature gradients exist with the wave-particle observations. The plasma parameters have been determined adequate to trigger the lower hybrid drift instability. The observation of β -dependence is consistent with drift-wave theories. Drift waves can also accelerate electrons along the magnetic field direction and form field-aligned beams that are unstable to cyclotron resonance instability, exciting whistler mode waves. These predicted features are all observed.

The wave-particle data come from the Plasma Electron And Current Experiment (PEACE) [11], the Composition Ion Spectrometry (CIS) instrument [12], the Flux Gate Magnetometer (FGM) experiment [13], the Spatio-Temporal Analysis of Field Fluctuation (STAFF) instrument [14] and the Waves of High frequency and Sounder for Probing of Electron density Relaxation (WHISPER) experiment [15].

Observations.—Of the nine events studied, the clearest case that shows the salient features of wave-particle relationships comes from observations made on 22 September 2004 (Fig. 1). Cluster 1 (CL1) was in the geomagnetic tail at a distance of $(-18, 4.14, -2.83)$ Earth radii (R_E) and detected ions with ~ 350 km s $^{-1}$ bulk speeds in $-V_x$ (tail) and $+V_y$ (dusk) directions (Fig. 1, panel 2). A magnetic structure was embedded within this flowing plasma as indicated by the variations of B_x (decrease) and B_y (increase) starting ~ 0342 U.T. (panel 3). Timing information from the four Cluster satellites indicates this structure was ~ 2200 km thick and tilted by $\sim 23^\circ$ from the ecliptic plane.

We distinguish three time intervals (R1, R2, and R3) corresponding to three different magnetic regimes. R1, characterized by $|B| \sim 8\text{--}12$ nT and $\beta_i \sim 1\text{--}6$ (panels 3–4), is

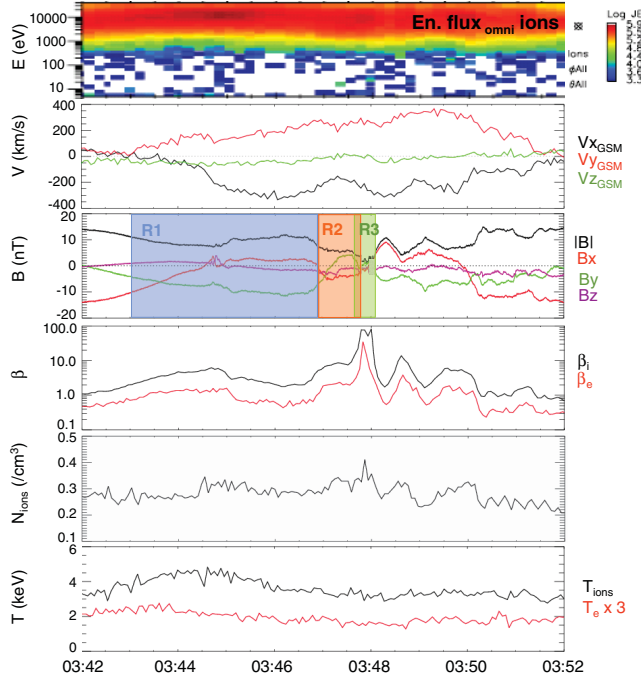


FIG. 1 (color). 22 September 2004 event: (1) Spectrogram of the ion energy flux. (2) Components of the ion bulk velocity. (3) B -field components and magnitude. (4) Ion (black) and electron (red) plasma beta. (5) Plasma density. (6) Ion (T_i) and electron ($T_e \times 3$) temperatures.

the plasma sheet boundary layer (PSBL). The density N in the PSBL is $\sim 0.28 \text{ cm}^{-3}$ (panel 5) and ion temperature $T_i \sim 4000 \text{ eV}$ (panel 6). The electron temperature is lower, $T_e \sim 700 \text{ eV}$. CL1 entered PSBL at $\sim 0343 \text{ U.T.}$ as the ion bulk speed increased.

At 0346:50 U.T., CL1 encountered a large B -field gradient and crossed into R2, the current sheet (CS), as indicated by change of signs in B_x and B_y . In R2, $|B| \sim 5\text{--}8 \text{ nT}$, $\beta_i \sim 10$, $N \sim 0.32 \text{ cm}^{-3}$, $T_i \sim 3000 \text{ eV}$ and $T_e \sim 500 \text{ eV}$.

Deeper in the CS, CL1 encountered a region R3 with $|B| < 5 \text{ nT}$, $\beta_i \sim 80$ and $\beta_e \sim 35$. The peak density $N \sim 0.4 \text{ cm}^{-3}$ and T_i remain nearly constant, indicating the high β_i is mainly due to the reduction in $|B|$ that nearly vanishes in the neutral sheet (NS).

Three kinds of emissions were detected (Fig. 2). In the PSBL (R1), the waves are essentially electrostatic (panel 1, 0343–0346:50 U.T.). In the CS (R2), the waves are purely electromagnetic (panels 2–3, 0346:50–0347:50 U.T.). At the edges of the NS (R3), only low frequency electromagnetic waves are present (panel 3). The low frequency magnetic field fluctuations were obtained by low pass filtering the FGM data. These are extremely large amplitude waves, peak values reaching $\sim 2 \text{ nT}$.

Phase space density parallel (f_{\parallel} , panel 4), perpendicular (f_{\perp} , panel 5), and antiparallel ($-f_{\parallel}$, panel 6) to \mathbf{B} show that the waves in R1 and R2 are associated with complex electron structures. We can see, for example, field-aligned

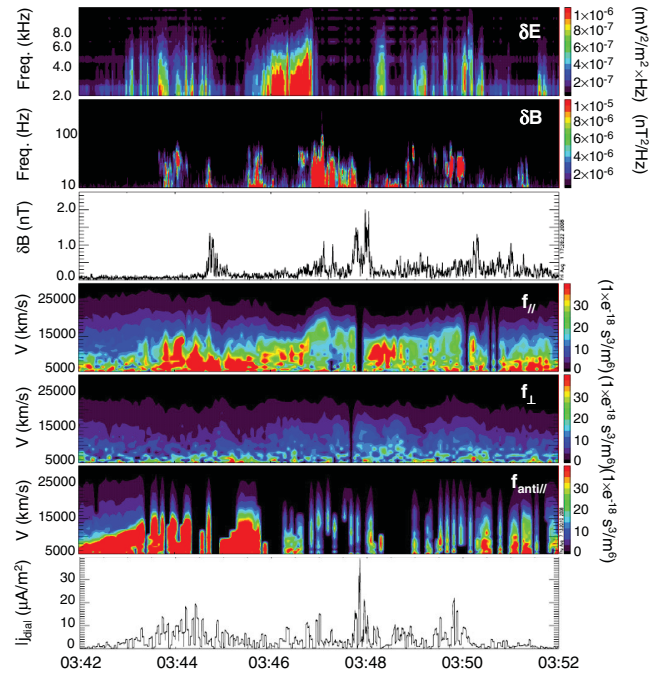


FIG. 2 (color). (1) Spectrogram of the electric field fluctuations (2–14 kHz). (2) Spectrogram of the high frequency (8–350 Hz) magnetic fluctuations. (3) Low frequency ($< 8 \text{ Hz}$) fluctuations of \mathbf{B} . (4–6) Spectrograms of the components of the electron distribution function parallel, perpendicular and antiparallel to \mathbf{B} . (7) Magnitude of the diamagnetic current density.

electron beams at discrete energies and speeds traveling in both directions of the magnetic field, differing considerably from those electrons in the perpendicular direction. The complex electron features are closely associated with ES and EM waves and they give important information about the plasma mechanisms active in these regions.

Counterstreaming electron beams and ES waves (0342:14–0346:50 U.T.).—Figure 3 shows 1D phase space plots of the electron distributions. In the PSBL, field-aligned electron beams stream parallel and antiparallel to \mathbf{B} through a hot ($\sim 700 \text{ eV}$) and isotropic Maxwellian plasma whose distribution is similar to those in the PS.

The speed (v_{\parallel}) of the beams increases linearly in time [Figs. 3(a)–3(d)]. Before CL1 entered the PSBL until $\sim 0343:30 \text{ U.T.}$, v_{\parallel} was $\sim 7000 \pm 100 \text{ km s}^{-1}$ ($\sim 70 \text{ eV}$). Deeper in the PSBL until 0346:45 U.T., v_{\parallel} increased to $\sim 12000 \pm 400 \text{ km s}^{-1}$ ($\sim 410 \text{ eV}$). The temperature T_{beam} of these beams varied between $10 \pm 1 \text{ eV}$ and $100 \pm 30 \text{ eV}$.

These beams are detected in coincidence with broadband ES waves in the frequency range 2–6 kHz (Fig. 2), close to the PSBL electron plasma frequency $f_{pe} \sim 5 \text{ kHz}$. These emissions contain the Langmuir waves and contributions from the unresolved Debye scale solitary structures that are prominent in the PSBL [6]. The ES waves could be produced by the nonlinear evolution of the electron acoustic and electron-ion instabilities initiated by the beams [16].

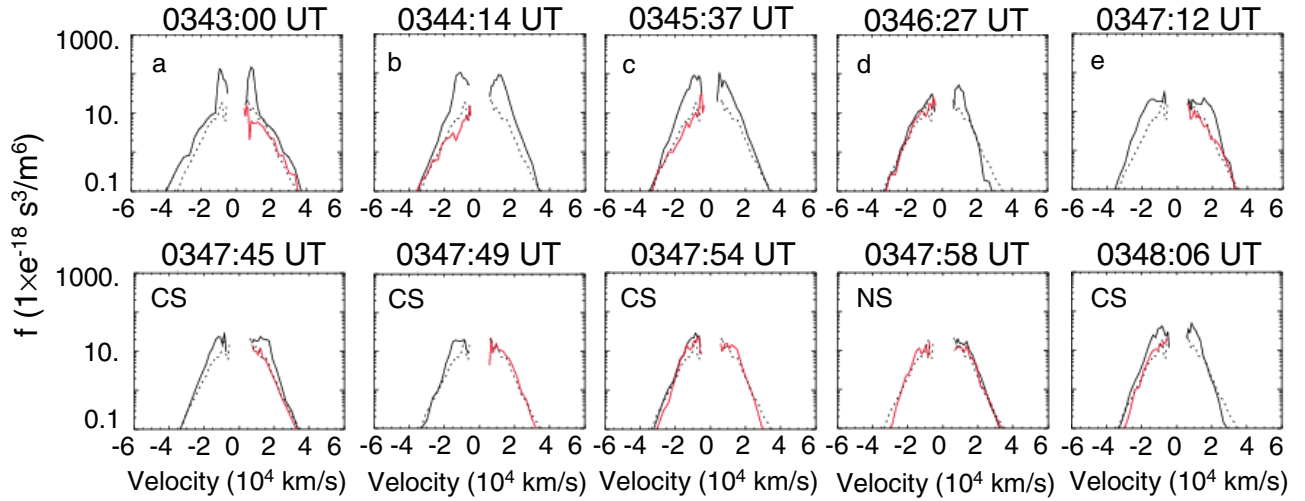


FIG. 3 (color). One-dimensional cuts of the electron distribution functions in the directions parallel ($v > 0$, black), antiparallel ($v < 0$, black) and perpendicular (red) to \mathbf{B} . The plasma sheet (PS) distribution function is shown as dotted lines.

Flat-top distributions and EM waves.—In the CS (0346:50–0347:50 U.T.), the electron distribution functions show a field-aligned flat-top shape [Fig. 3(e)]. Such distributions seen throughout the CS have a cutoff speed around $\sim 15\,000$ – $17\,000$ km s^{-1} . Some of them can be represented by a combination of two Gaussians with $T_{\text{beam}} \sim 30 \pm 10$ eV and $T_{\text{beam}} \sim 100 \pm 60$ eV.

These distributions are observed concurrently with purely EM waves at ~ 10 – 80 Hz ($<$ the electron cyclotron frequency $f_{ce} \sim 170$ Hz in this region). These EM emissions are whistler mode waves that are detected often in the plasma sheet [9] at frequencies 0.05 – $0.5 f_{ce}$ [17]. Low frequency (< 2 Hz) EM waves are also detected in the region where the plasma density showed a positive gradient (panel 5, Fig. 1) and the ion and electron temperatures negative gradients (panel 6).

Isotropic distribution and weak low frequency Alfvén waves (0347:42–0348:04 U.T.).—The second row of Fig. 3 displays electron distributions taken at 5 times, at the edge and in and just outside of the NS. The first three panels show how the flat tops progressively disappear between 0347:45 and 0347:54 U.T., when $|B|$ decreases from ~ 3.5 to 1.5 nT as CL1 approaches the neutral sheet (NS). Inside the NS, the electron distribution is isotropic (0347:58 U.T.), similar to those seen in the PS. At the edges of the NS, two bursts of EM waves with frequencies < 2 Hz are observed (panel 3, Fig. 2). These are similar to those seen in the CS, but with much stronger intensities and occur in regions of strong magnetic and density gradients.

Minimum variance analysis of these low frequency waves reveals two different normalized wave vectors $\mathbf{k}/|k|$, $(-0.50; -0.69; 0.52)$ and $(-0.08; -0.54; -0.84)$. The angle between \mathbf{k} and \mathbf{B} varies from 85° to 105° during the first time interval. It then changes to $\sim 55^\circ \pm 15^\circ$. Thus, \mathbf{k} is nearly perpendicular to \mathbf{B} for the first burst and oblique for the second.

The phase speeds of these waves in the plasma frame are determined, respectively, as 157 ± 71 km s^{-1} and 320 ± 192 km s^{-1} . The speed of the first wave is comparable to the Alfvén speed, $V_A = B/(\mu_0 N m_i)^{1/2} \sim 116$ km s^{-1} and smaller than the sound speed ($V_s = [k_B(T_e + T_i)/m_i]^{1/2} \sim 620$ km s^{-1}) while the speed of the second wave varied considerably during the observation, resulting in large uncertainties. These waves have frequencies less than the lower hybrid (LH) frequency ~ 1.5 – 2 Hz at that time.

These are compressional Alfvén waves that propagate perpendicular and obliquely to \mathbf{B} . High frequency ES waves are not observed in the NS. Neither are the high frequency whistler mode EM waves that are totally absent from 0347:48 to 0348:02 U.T. Typical plasma parameters characterizing these regions are summarized in Table I.

Discussion.—Three features important for identifying the wave-particle interaction mechanisms are: (i) the association of ES waves in the PSBL with cold field-aligned counterstreaming beams flowing through the hot isotropic Maxwellian plasma. These signatures are different from the usual theories that consider ES waves to be excited by gentle beams and two-stream instabilities with a bump-in-tail configuration, where the beam is hot and the back-

TABLE I. Plasma parameters in R1, R2, and R3.

	R1	R2	R3
B (nT)	8–12	5–8	< 5
β	1–6	10	10–80
n (cm^{-3})	0.27–0.32	0.29–0.34	0.34–0.41
T_e (eV)	600–800	~ 500	~ 500
T_i (keV)	3.7–5.0	~ 2.8 – 3.0	~ 2.8
V_b (km s^{-1})	7000–12 000	15 000–17 000	~ 0 .
T_b (eV)	10–100	30–100	~ 0 .
Waves	ES	EM whistler and Alfvén	\sim none
Frequencies	~ 2 – 6 kHz	10–80 Hz and < 2 Hz	—

ground electron population is cold [6,18], (ii) the association of flat-top electron distributions with EM whistler mode waves and low frequency Alfvén waves with frequencies less than the lower hybrid frequency (f_{lh}) in the CS regions with large plasma density and B -field gradients, and (iii) observations of only low frequency Alfvén waves at the edge of the NS where strong B -field and N gradients exist. The Alfvén and whistler mode waves damp out deep in the NS where plasma $\beta \sim 100$.

The plasma gradients contribute to the diamagnetic current $\mathbf{j}_{dia} (= \mathbf{B} \times \nabla_{\perp} P_{\perp} / B^2$, where P_{\perp} is the total perpendicular pressure) shown in panel 7 of Fig. 2. Such currents can destabilize the lower hybrid drift instability (LHDI). The LHDI can then trigger low frequency whistler mode waves propagating parallel and perpendicular to \mathbf{B} with frequencies close to f_{lh} [18], also called low frequency Alfvén waves. Thus, we suggest that the low frequency ($\sim 0.4 \text{ Hz} < f_{lh}$) Alfvén waves observed in the CS and at the edges of the NS propagating obliquely to \mathbf{B} are produced by the LHDI initiated by density and temperature gradients.

The LHD waves can also accelerate electrons in the parallel and antiparallel directions, producing field-aligned beams and flat-top shape distributions when the wavelength is sufficiently long [19,20]. The simultaneous observations of the low frequency Alfvén waves and flat-top electron distributions indicate that such a wave-particle interaction had occurred. Moreover, the detection of whistler mode waves indicates that the electron beams were unstable to the electron cyclotron instability, triggering the cyclotron mode waves. In regions of increasing β and strong B -field gradient, the waves interact less with the electrons. Indeed, the flat-top electron distributions there started to disappear while the low frequency Alfvén waves were still intense. Moreover, strong B -field gradients can increase the propagation angle of the whistler mode waves, enhancing Landau damping [17]. The absence of such waves in the NS suggests that the strong B -field gradients prevented them from propagating from the CS. It further signifies that these waves were not generated within the NS. This region had high plasma $\beta \sim 80$ and the LHDI was quenched, weakening the compressional Alfvén waves and preventing the formation of any beams that trigger the whistler mode waves.

Drift-wave instabilities resulting from a density, temperature or magnetic field gradient in a two component and finite but low $\beta (\ll 1)$ plasma have been studied for waves with frequencies $\omega \ll \omega_{ci}$ (ω_{ci} is the ion cyclotron frequency) [21,22]. The two plasma populations considered were, respectively, dense and cold and tenuous and hot, opposite to what we observed. The influence of a density gradient whether accompanied or not with temperature or \mathbf{B} curvature or shear effects has also been studied, again for plasma $\beta \ll 1$ [23]. These theories are not applicable to

our observations and thus quantitative estimates of the growth rates or detailed comparisons with our data must await until a drift-wave theory is available for plasmas with $\beta \sim 10\text{--}100$. Future research plan will focus on modeling our observations with particle simulation codes to understand the details of the mechanisms.

We acknowledge the Cluster Active Archive for the electron and fields data and are grateful to M. Wilber, E. Lee, N. Lin, and M. Fillingim for their helpful discussions and constructive remarks. The research at UC Berkeley is performed under NASA Grant No. NNG04GF23G.

*ateste@ssl.berkeley.edu

- [1] J. McFadden *et al.*, *Geophys. Res. Lett.* **25**, 2045 (1998).
- [2] G. Parks, L. J. Chen, M. Fillingim, M. McCarthy, *Space Sci. Rev.* **95**, 237 (2001).
- [3] R. Treumann and T. Terasawa, *Space Sci. Rev.* **99**, 135 (2001).
- [4] J. Arons, in *General Relativistic Polar Particle Acceleration and Pulsar Death* (Universal Academy Press, Tokyo, 1998), p. 339.
- [5] P. Canu, *J. Geophys. Res.* **94**, 8793 (1989).
- [6] H. Matsumoto, H. Kojima, T. Miyatake, Y. Omura, M. Okada, I. Nagano, and M. Tsutsui, *Geophys. Res. Lett.* **21**, 2915 (1994).
- [7] K. R. Lang, *Astrophys. J., Suppl. Series* **90**, 753 (1994).
- [8] V. N. Oraevsky, Iu. Ia. Ruzhin, and S. Dokukin, *Adv. Space Res.* **12**, 43 (1992).
- [9] D. A. Gurnett, L. A. Frank, and R. P. Lepping, *J. Geophys. Res.* **81**, 6059 (1976).
- [10] I. Shinohara, T. Nagai, M. Fujimoto, T. Terasawa, K. Tsuruda, and T. Yamamoto, *J. Geophys. Res.* **103**, 20365 (1998).
- [11] A. D. Johnstone *et al.*, *Space Sci. Rev.* **79**, 351 (1997).
- [12] H. Rème *et al.*, *Ann. Geophys.* **19**, 1303 (2001).
- [13] A. Balogh *et al.*, *Space Sci. Rev.* **79**, 65 (1997).
- [14] N. Cornilleau-Wehrlin *et al.*, *Ann. Geophys.* **21**, 437 (2003).
- [15] P. M. E. Décréau *et al.*, *Ann. Geophys.* **19**, 1241 (2001).
- [16] D. Schriver and M. Ashour-Abdalla, *Geophys. Res. Lett.* **16**, 899 (1989).
- [17] Y. Zhang, H. Matsumoto, and H. Kojima, *J. Geophys. Res.* **104**, 28633 (1999).
- [18] R. Treumann and W. Baumjohann, *Advanced Space Plasma Physics* (Imperial College Press, London, 1997).
- [19] N. Dubouloz, R. A. Treumann, R. Pottelette, and K. A. Lynch, *Geophys. Res. Lett.* **22**, 2969 (1995).
- [20] I. Shinohara and M. Hoshino, *Adv. Space Res.* **24**, 43 (1999).
- [21] A. Hasegawa, *Phys. Rev. Lett.* **27**, 11 (1971).
- [22] S. Ichimaru, *Basic Principles of Plasma Physics* (W.A. Benjamin Inc., Reading, 1973), p. 187.
- [23] N. A. Krall and M. N. Rosenbluth, *Phys. Fluids* **8**, 1488 (1965).